

Modeling and Simulation of Simplified Quadruple Diode Solar PV Module Under Influence of Environmental Conditions and Parasitic Resistance

Ali M. Jasim¹, Baraa M. Albaker², Hussein Jumma Jabir²

¹Department of Network Engineering, College of Engineering, Aliraqia University, Baghdad, Iraq

²Department of Electrical Engineering, College of Engineering, Aliraqia University, Baghdad, Iraq

Abstract – To ensure a rapid and consistent design of Photovoltaic (PV) modules, the presence of an effective simulator is essential for assessing the behaviour of the PV cell when subjected to rapid or partial changes in temperature, irradiance, and parasitic resistance. The prevailing approach for modelling involves utilizing an equivalent circuit that encapsulates both nonlinear and linear mechanisms. The study introduces an eleven-parameter quartic model for the simulation and modelling of a PV unit. The model takes into account the equivalent circuit constraints of the PV cell and validated by solving the non-linear voltage equation. The examination concentrates on three pivotal junctures: open circuit, maximum power point, and short circuit. These key points are crucial for comprehending the operational characteristics of the PV module in typical conditions. The proposed quadruple diode model has been demonstrated to outperform the lower-order diode models in terms of performance and accuracy.

To validate the strength and precision of the developed model, the model was simulated using the specifications of PV panels, and the outcomes were compared with the recorded values obtained from the lower-order models. The model was developed and tested using standard mathematical equations for PV cells within the MATLAB/ Simulink environment.

Keywords – PV, modelling and simulation, quadruple-diode model, temperature and irradiance, parasitic resistance.

1. Introduction

The progress of civilization marked by an extraordinary revolution in energy technology has brought to light several environmental issues and crises, including global warming, air pollution and ozone layer depletion, etc. [1], [2]. Countries worldwide are prioritizing the adoption of renewable and infinite energy sources to attain clean and sustainable energy. These sources include Photovoltaic (PV) systems, wind turbines, gravitational energy, biomass energy, hydropower and geothermal energy, and more [3], [4], [5]. Among these options, solar energy has emerged as a highly viable and promising alternative. It is abundant, boasts reasonable efficiency, and entails low maintenance costs. Solar power technology has experienced remarkable progress in recent times, establishing itself as a leading contender in the renewable energy domain. Embracing solar energy presents tremendous potential for fostering a cleaner and more sustainable living environment for our planet.

Accurate prediction of the performance of a PV cell under varying environmental conditions, including solar temperature, and generating power-voltage and current-voltage curves require modeling and consideration of parasitic resistance [6].

DOI: 10.18421/TEM131-79

<https://doi.org/10.18421/TEM131-79>

Corresponding author: Ali Mahmood Jasim,
Department of Network Engineering, College of Engineering, Aliraqia university, Sab'abkar, 10054, Baghdad, Iraq


Email: drali7819@gmail.com

Received: 11 October 2023.

Revised: 06 February 2024.

Accepted: 13 February 2024.

Published: 27 February 2024.

 © 2024 Ali M. Jasim, Baraa M. Albaker & Hussein Jumma Jabir; published by UIKTEN. This work is licensed under the Creative Commons Attribution-NonCommercial-NoDerivs 4.0 License.

The article is published with Open Access at <https://www.temjournal.com/>

A commonly used method involves employing an equivalent electrical circuit that combines both linear and nonlinear components. Relying solely on the specifications of the PV solar panel, which provides limited specifications like open circuit voltage (VOC), short circuit current (ISC), maximum voltage (VMPP), maximum current (IMPP), and maximum power point (PMPP) at standard operating conditions (SOC), is insufficient for precise modeling [7], [8], [9]. PV cells operate under various irradiance and temperature conditions, demanding a deeper understanding of their nonlinear current-voltage specification and the parameters modification based on data provided by the PV solar panel.

Numerous researchers have proposed multiple models to precisely simulate PV cells. These models encompass various configurations, such as the single diode model (SDM) [10], double diode model (DDM) [11], triple diode model (TDM) [12], and quadruple diode model (QDM) [13]. Each of these PV models aims to accurately represent the electrical behavior of the cell. The simplest diode modelling is the single diode model that has one diode. Higher-order models, including double, triple and quadruple diodes, have linear and nonlinear elements with additional diodes to accurately capture the PV cell's electrical behavior. Therefore, these models represent an important role in forecasting the performance of PV cells under wide environmental conditions. This will result in improving the precision and efficiency of the PV systems.

The addition of a fourth diode that is connected in parallel with the third diode will result in enhancing lower-order model versions in terms of the reliability and performance of the solar module under wide operating conditions. The resulting higher accuracy model is called the four-diode model. Even though the four-diode models provide higher accuracy, additional diodes increase system complexity and requires higher computational demands [14], [15]. The main goal is therefore to extract a simplified solar model that encapsulates the model constraints and assesses the behavior of the PV while maintaining adequate computational power requirement with high efficiency.

The major contribution of this research is to extract an extensive quadruple diode model for a PV cell by simplifying and restructuring the current equation through minimizing constraints to nine equations. The performance of the developed model is then compared to single diode model and multiple diode models. As a result, the extracted model has a significant value to build models and study the characteristics of PV modules. Such research that uses the developed model may be conducted for instance in optimization of energy storage devices, power converters design, and maximum power point trackers.

Therefore, the proposed model acts as an important tool to model and simulate the behavior of the PV modules with high accuracy, accordingly allowing effective solar energy harnessing.

The installation size of PV systems is notably increasing in the future, as clearly declared in the current researches [16], [17]. This is because of the nonlinearity behavior of PV cells due to several environmental issues such as radiation and temperature. Thus, highly accurate PV cell modelling is a challenging task. Hence, PV cell modelling that used to accurately and precisely compute the output power while counting for different operating condition becomes crucial issue. This has led to extracting different models for PV cells, including single, double, triple, and quadruple models, each offering unique insights into the behavior of PV systems.

2. Modelling PV Cells

The use of mathematical modeling for photovoltaic cells, modules, and arrays is essential to comprehend, analyze, and anticipate the performance of solar PV systems amidst various environmental conditions and operational variables. The following subsections list various types of the PV models.

2.1. Single Diode Model

The SDM, depicted in Figure 1, is a traditional PV model that includes one diode connected with a light-generated current source I_{ph} in parallel, alongside a series resistance R_{se} and a parallel admittance G_{pa} (where $G_{pa}=1/R_{pa}$) [18]. This model, called five parameters model, comprises I_{ph} , I_{rs} , n , R_{se} , and R_{pa} [19], [20], [21]. Although it offers advantages, its accuracy diminishes when irradiance levels decrease. Utilizing Kirchhoff's Current Law (KCL), the model calculates the output current I_{PV} using Equation 1. Nomenclature of all variables used in this research is depicted in Appendix A.

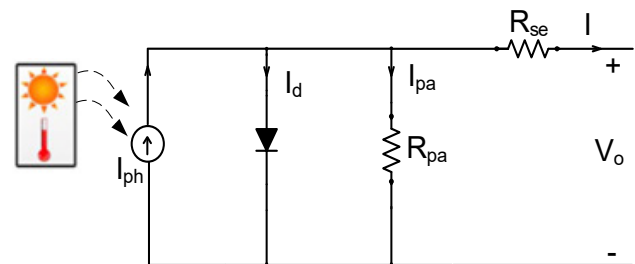


Figure 1. Single diode model's equivalent circuit diagram

$$I = I_{ph} - I_{rs} \left[\exp \left(\frac{V_o + IR_{se}}{nV_T} \right) - 1 \right] - G_{pa}(V_o + IR_{se}) \quad (1)$$

The single diode equivalent circuit model for solar PV cells has several benefits, such as its straightforward control structure and minimal circuit complexity. However, it also has limitations, including subpar accuracy and irregular output characteristics. Despite these drawbacks, the model continues to be extensively utilized in the solar PV industry, particularly in applications that demand quick response times.

2.2. Double Diode Model

In this modified model, another diode is connected in parallel with the existing diode, while the rest of the circuit remains unchanged [22], [23]. This configuration is depicted in Figure 2. The DDM equivalent circuit model is a variation of the SDM equivalent circuit model, incorporating two reverse saturation currents (I_{rs1} , I_{rs2}), two ideality factors (n_1, n_2), and the diode currents represented as I_{d1} and I_{d2} . The output current (I), is defined by Equation 2.

Compared to the single diode model, the DDM presents several advantages. It offers improved accuracy in fitting curves and exhibits satisfactory performance under standard test conditions (STC). The DDM's equivalent circuit includes seven parameters to estimate, namely I_{ph} , I_{rs1} , I_{rs2} , n_1 , n_2 , R_{se} and G_{pa} . The DDM is commonly employed in practical scenarios where higher accuracy in output current-voltage (I-V) characteristics is needed, especially in low irradiation conditions and situations requiring adaptability to varying environmental conditions [24].

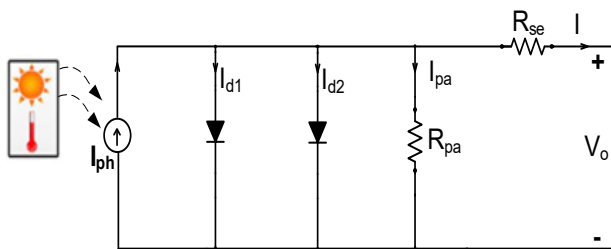


Figure 2. Double diode model's equivalent circuit diagram

$$I = I_{ph} - I_{rs1} \left[\exp \left(\frac{V_o + IR_{se}}{n_1 V_T} \right) - 1 \right] - I_{rs2} \left[\exp \left(\frac{V_o + IR_{se}}{n_2 V_T} \right) - 1 \right] - G_{pa}(V_o + IR_{se}), \quad (2)$$

2.3. Triple Diode Model

The TDM [25], [26] represents an advanced enhancement over the DDM and introduces further improvements.

The TDM equivalent circuit of PV solar cells utilizes three diodes, as illustrated in Figure 3. The third diode, I_{d3} , is connected in parallel with first and second diodes, I_{d1} and I_{d2} , respectively. The TDM accounts for the influence of grain boundaries and leakage current, which are represented by I_{d3} . The flow of leakage current occurs through the parallel resistance in the triple equivalent circuit model [26].

The TDM is presented in Equation 3. It incorporates three diodes within the model [27],[28]. Nine parameters are required by the triple model to fully characterize its I-V characteristic, which are: I_{rs2} , I_{rs3} , I_{ph} , I_{rs1} , n_1 , n_2 , n_3 , G_{pa} and R_{se} . The model offers a remarkable level of accuracy for a solar PV cell in curve fitting, mainly in challenging conditions like higher temperatures and lower irradiance. Also, precise identification of various current components can be obtained within the cell. Nevertheless, it is crucial to categorize that the model is of high complexity. The common use of the model is in large-scale industrial silicon solar cells to accurately present the I-V characteristics and accordingly predict the generated power with high accuracy.

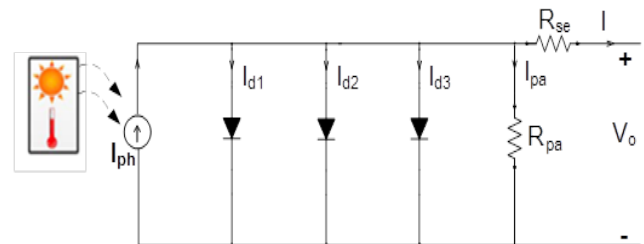


Figure 3. Triple diode model's equivalent circuit diagram

$$I = I_{ph} - I_{rs1} \left[\exp \left(\frac{V_o + IR_{se}}{n_1 V_T} \right) - 1 \right] - I_{rs2} \left[\exp \left(\frac{V_o + IR_{se}}{n_2 V_T} \right) - 1 \right] - I_{rs3} \left[\exp \left(\frac{V_o + IR_{se}}{n_3 V_T} \right) - 1 \right], \quad (3)$$

2.4. Quadruple Diode Model

The QDM, in contrast to lower-order diode models, offers numerous advantages, particularly for industrial solar PV cells. The model offers minimized difference between actual and estimated data and increased accuracy. This in turn resulting in model superiority as compared to other models in terms of accuracy for curve fitting. Additionally, the quadruple diode model performs exceptionally well in standard test conditions (STC). However, it is important to acknowledge that this model comes with the drawback of higher complexity in terms of modeling. Despite its complexity, the quadruple diode model is widely used in large-scale industrial applications [13].

The fourth diode, I_{d4} , is connected in parallel with the constant current source of the first, second and third diodes, I_{d1} , I_{d2} , and I_{d3} , respectively. Figure 4 depicts the equivalent circuit diagram of the quadruple model. The model introduces two additional constraints that need to be taken into account during the modeling process: the reverse saturation diode current I_{rs4} and the ideality factor n_4 . Thus, the total number of constraints becomes eleven for the quadruple model. These constraints include the light-generated current source I_{ph} , diode saturation currents I_{rs1} , I_{rs2} , I_{rs3} and I_{rs4} , ideality factors of the diodes n_1 , n_2 , n_3 , and n_4 , series resistance R_{se} , and parallel admittance G_{pa} . The quadruple model is mathematically represented as given in Equation (4), and the currents through diodes 1, 2, 3, and 4 are expressed by Equations (5), (6), (7), and (8) respectively.

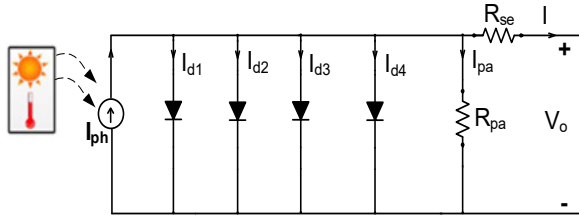


Figure 4. Quadruple diode model's equivalent circuit diagram

$$I = I_{ph} - I_{d1} - I_{d2} - I_{d3} - I_{d4} - G_{pa}(V_o + IR_{se}), \quad (4)$$

$$I_{d1} = I_{rs1} \left[\exp\left(\frac{V_o + IR_{se}}{n_1 V_T N_{se}}\right) - 1 \right] \quad (5)$$

$$I_{d2} = I_{rs2} \left[\exp\left(\frac{V_o + IR_{se}}{n_2 V_T N_{se}}\right) - 1 \right] \quad (6)$$

$$I_{d3} = I_{rs3} \left[\exp\left(\frac{V_o + IR_{se}}{n_3 V_T N_{se}}\right) - 1 \right] \quad (7)$$

$$I_{d4} = I_{rs4} \left[\exp\left(\frac{V_o + IR_{se}}{n_4 V_T N_{se}}\right) - 1 \right] \quad (8)$$

Substituting Equations (5), (6), (7), and (8) into Equation (4) and rephrasing it to yield Equation (9). Also, the thermal voltage V_T of the PV cell can be mathematically expressed using Equation (10).

$$I = I_{ph} - \sum_{i=1}^4 I_{rsi} \left[\exp\left(\frac{V_o + IR_{se}}{n_i V_T N_{se}}\right) - 1 \right] - G_{pa}(V_o + IR_{se}), \quad (9)$$

$$V_T = \frac{K_B T_{op}}{q} \quad (10)$$

3. Mathematical Modelling of Quadruple Diode PV Cell

The process of mathematical modeling quadruple diode PV cells entails creating sophisticated models that precisely depict the electrical characteristics of the cells. While single, double, and triple diode models are prevalent and thoroughly investigated, the quadruple diode model presents a more intricate and refined method for characterizing the behavior of PV cells across diverse environmental conditions.

3.1. Determination of I_{ph} Photocurrent Model

The photocurrent mostly is a function of the working temperature and solar isolation of the PV cell [10], [11]. Figures 5 and 6 illustrate internal and external photocurrent model block diagram. It acts as a subsystem in the development of solar cell model as represented by Equation (11).

$$I_{ph} = \frac{G_{ir}}{G_{STC}} [I_{sc_STC} + K_{sc} (T_{op} - T_{ref})] \quad (11)$$

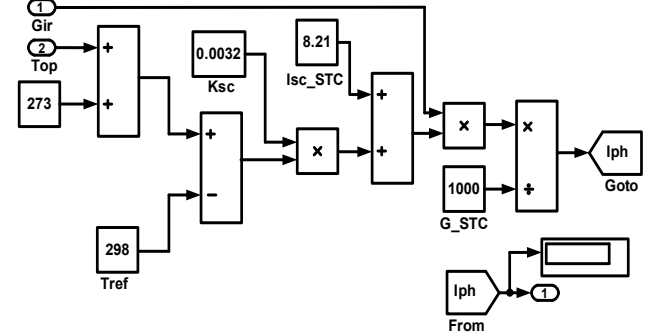


Figure 5. Equivalent circuit diagram of photocurrent Model

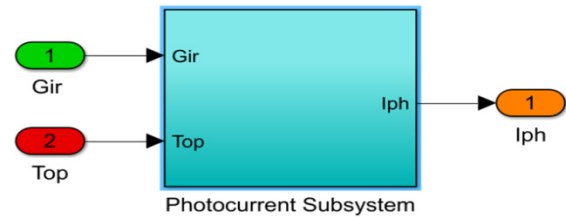


Figure 6. Photocurrent subsystem

3.2. Determination of I_{rs} Reverse Saturation Current Model

Diode reverse saturation current (I_{rs}) depends on the temperature coefficient, which includes (K_{sc}) and (K_{ov}). For the single model, an improved formula used to define the diode reverse saturation current with varying temperature values is illustrated in Equation (12) [22]. Figures 7 and 8 respectively represent the internal and external block diagram of diode reverse saturation current. It acts as a subsystem in solar cell model as illustrated by Equation (12).

$$I_{rs} = \frac{I_{sc_STC} + K_{sc}(T_{op} - T_{ref})}{\exp(V_{oc_STC} + K_{ov}(T_{op} - T_{ref})/nV_T) - 1} \quad (12)$$

The inputs of diode reverse saturation current are operating temperature (Kelvin) and short circuit current (A). The output of the subsystem is the diode reverse saturation current (A). The block covers the following parameters: open circuit voltage at standard condition (V_{oc_STC}), electron charge (q), Boltzmann constant (K_B), number of series cells (N_{se}), and diode ideality factor (n).

To simplify the analysis and simulation of a PV module using a four-diode model, the diode reverse saturation current equation can be expressed in terms of the open circuit voltage temperature coefficient (K_{OV}), as shown in Equation (13). However, the process of developing the four-diode model involves the need to estimate eleven constraints, leading to increased complexity in the analysis and making the simulation of the PV module less straightforward.

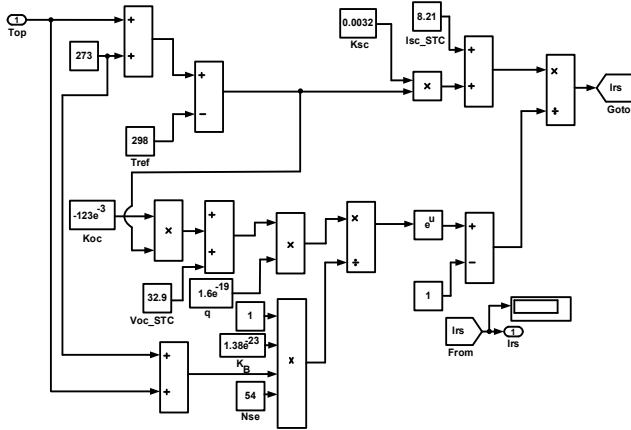


Figure 7. Equivalent circuit diagram of reverse saturation current model

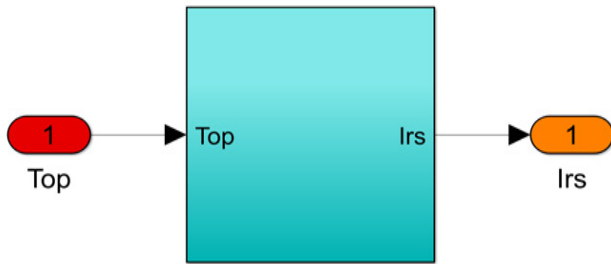


Figure 8. Diode reverse saturation subsystem

$$I_{rs} = I_{rs1} = I_{rs2} = I_{rs3} = I_{rs4} = \frac{I_{sc_STC} + K_{sc}(T_{top} - T_{ref})}{\exp\left(\frac{V_{oc_STC} + K_{ov}(T_{top} - T_{ref})}{V_T(n_1 + n_2 + n_3 + n_4/P)}\right) - 1} \quad (13)$$

To simplify the model and enhance its manageability, researchers have successfully reduced the original eleven constraints to five, as detailed in Equation (9). This reduction of constraints can also be implemented when constructing the four-diode model. In order to facilitate the analysis, the following assumptions have been taken into consideration: $I_{rs} = I_{rs1} = I_{rs2} = I_{rs3} = I_{rs4}$ and $(n_1 + n_2 + n_3 + n_4/P) = 1$.

By plugging in the irradiance and temperature inputs into Equations (11) and (14), the diode saturation currents and photocurrent are calculated with the data supplied by the specifications of PV panels.

In order to achieve optimal results in the PV cell module for current-voltage curve, the ideality factors n_1, n_2, n_3 and n_4 are assigned specific values. Specifically, n_1 is set to 0.3, n_2 is set to 0.5, n_3 is set to 0.7, and n_4 is set to 1. It is advisable to select a value for P that exceeds 2. These modifications make the four-diode model more straightforward and appealing for PV module simulation. This is because only five constraints need to be calculated. Thus, the changes mentioned above simplify the four-diode model, making it an attractive option for PV system simulation.

$$I_{rs} = I_{rs1} = I_{rs2} = I_{rs3} = I_{rs4} = \frac{I_{sc_STC} + K_{sc}(T_{top} - T_{ref})}{\exp[V_{oc_STC} + K_{ov}\Delta T]/V_T} - 1 \quad (14)$$

3.3. Determination of I_s Saturation Current Model

The diode saturation current (I_s) depends on the temperature and the band-gap energy of the semiconductor material (E_g) [29], which can be described as Equation (15). Figures 9 and 10 respectively represent the internal and external diagram of the diode saturation current model and act as a subsystem in solar cell model as demonstrated in Equation (14).

$$I_s = I_{rs} \cdot \left(\frac{T}{T_{ref}}\right)^3 \cdot \exp\left[\frac{qE_g}{nK_B} \left(\frac{1}{T_{ref}} - \frac{1}{T_{top}}\right)\right] \quad (15)$$

The inputs of saturation current are operating temperature (Kelvin) and diode reverse saturation current (A). The circuit output is the diode saturation current (A). The block diagram covers the following parameters: electron charge (q), band-gap energy of the semiconductor material (E_g), diode ideality factor (n), and Boltzmann constant (K_B).

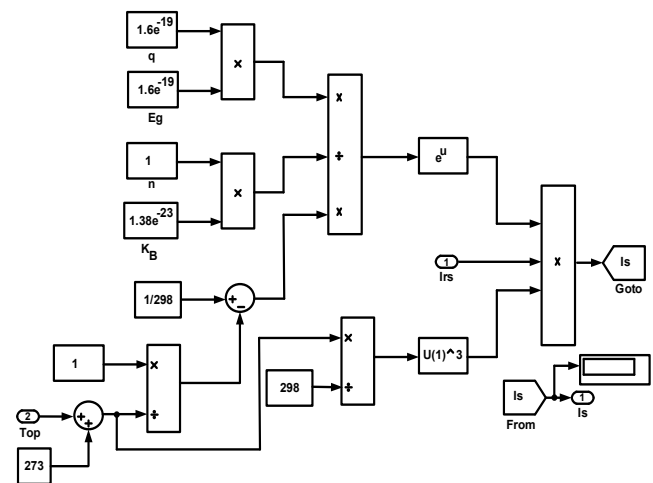


Figure 9. Equivalent circuit diagram of saturation current model

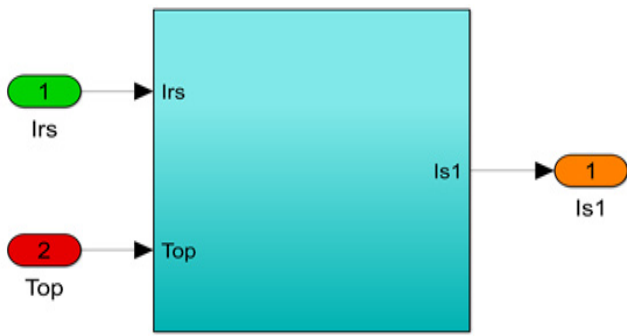


Figure 10. Diode saturation subsystem

3.4. Determination of Series R_{se} and Parallel R_{pa} Resistances

Numerous analytical and numerical methods proposed in the literature [10], [11] have been suggested to assess the constraints of PV cell models of one, two, and three diodes. The series resistance (R_{se}) and parallel resistance (R_{pa}) values can be determined through mathematical approaches [18].

The key task is to determine the appropriate values of (R_{se}) and (R_{pa}) such that the calculated power (P_{mpp} , C_a) matches the experimental power (P_{mpp} , Ex) provided by the manufacturer's data sheet. Figure 11 depicts the flowchart outlining the iterative process for adjusting the current-voltage curve. The iteration starts with $R_s = 0$ and continues to vary until the calculated maximum power (P_{mpp} , C_a) matches the experimental power (P_{mpp} , Ex), while (R_{pa}) simultaneously calculating the value of (R_{pa}). By adjusting (R_{se}) and (R_{pa}), it ensures that only one pair (R_{se} , R_{pa}) guarantees $(P_{mpp}, C_a) = (P_{mpp}, Ex) = V_{mpp} * I_{mpp}$ at the maximum power point on the current-voltage curve.

The expression for the light-generated current source under three different operating conditions, such as short circuit current (I_{sc}), open circuit voltage (V_{oc}) and maximum power point (V_{MPP}). During the open circuit condition, the voltage drop across the diode when the generated current, (I) is equal to zero and (V_o) is equal to (V_{oc_STC}). Substituting these values into the Equation (9), the light-generated current is derived as follows:

$$0 = I_{ph} - \sum_{i=1}^4 I_{rsi} \left[\exp\left(\frac{V_{oc_STC}}{n_i V_T Nse}\right) - 1 \right] - \frac{V_{oc_STC}}{R_{pa}}, \quad (16)$$

$$I_{ph} = \sum_{i=1}^4 I_{rsi} \left[\exp\left(\frac{V_{oc_STC}}{n_i V_T Nse}\right) - 1 \right] - \frac{V_{oc_STC}}{R_{pa}}, \quad (17)$$

During the short circuit condition, the greatest value of the current extracted in a PV cell, which is produced by the short circuit condition, (V_o) is equal to zero and (I) is equal to (I_{sc_STC}). Substituting these values into the Equation (9), the light-generated current is derived as follows:

$$I_{sc_STC} = I_{ph} - \sum_{i=1}^4 I_{rsi} \left[\exp\left(\frac{I_{sc_STC} R_{se}}{n_i V_T Nse}\right) - 1 \right] - \frac{I_{sc_STC} R_{se}}{R_{pa}}, \quad (18)$$

During the maximum operating condition, the operating point extracted by the solar cell at a point of the current-voltage characteristic where the product VI is maximized. (V_o) is equal to (V_{MPP_STC}) and (I) is equal to (I_{MPP_STC}). Substituting the above values into the Equation (9), the output current is derived as follows:

$$I_{MPP_STC} = \frac{I_{ph} - \sum_{i=1}^4 I_{rsi} \left[\exp\left(\frac{V_{MPP_STC} + I_{MPP_STC} R_{se}}{n_i V_T Nse}\right) - 1 \right] - \frac{V_{MPP_STC} + I_{MPP_STC} R_{se}}{R_{pa}}}{R_{pa}}, \quad (19)$$

$$\frac{V_{MPP_STC} + I_{MPP_STC} R_{se}}{R_{pa}} = \frac{I_{ph} - \sum_{i=1}^4 I_{rsi} \left[\exp\left(\frac{V_{MPP_STC} + I_{MPP_STC} R_{se}}{n_i V_T Nse}\right) - 1 \right]}{R_{pa}}, \quad (20)$$

The iteration process enables the estimation of the values of R_{se} and R_{pa} by utilizing equation (21).

$$R_{pa} = \frac{V_{MPP_STC} + I_{MPP_STC} R_{se}}{I_{ph} - \sum_{i=1}^4 I_{rsi} \left[\exp\left(\frac{V_{MPP_STC} + I_{MPP_STC} R_{se}}{n_i V_T Nse}\right) - 1 \right]} \quad (21)$$

4. Simulation Design of Quadruple Diode Model

The developed four-diode model is simulated using MATLAB/Simulink software through utilizing Equations (9), (11), (13), and (14) in the simulation process. Figure 11 illustrates the overall simulation model of the four-diode model. The major subsystems of the proposed four diode model and its module output current of the four diode PV cell are as shown in Figures 12, 13 respectively.

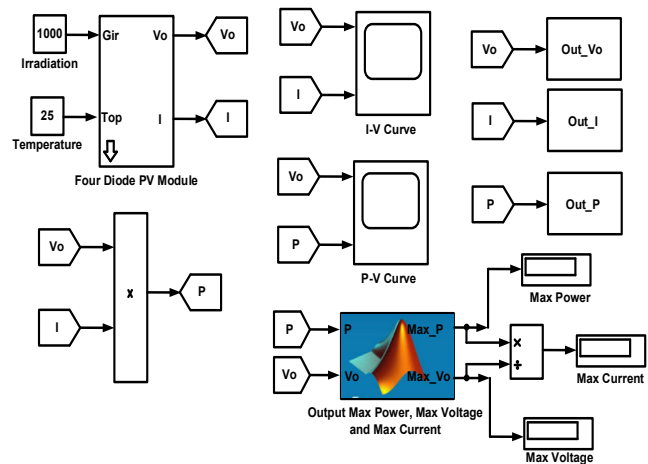


Figure 11. Overall PV of proposed four diode model

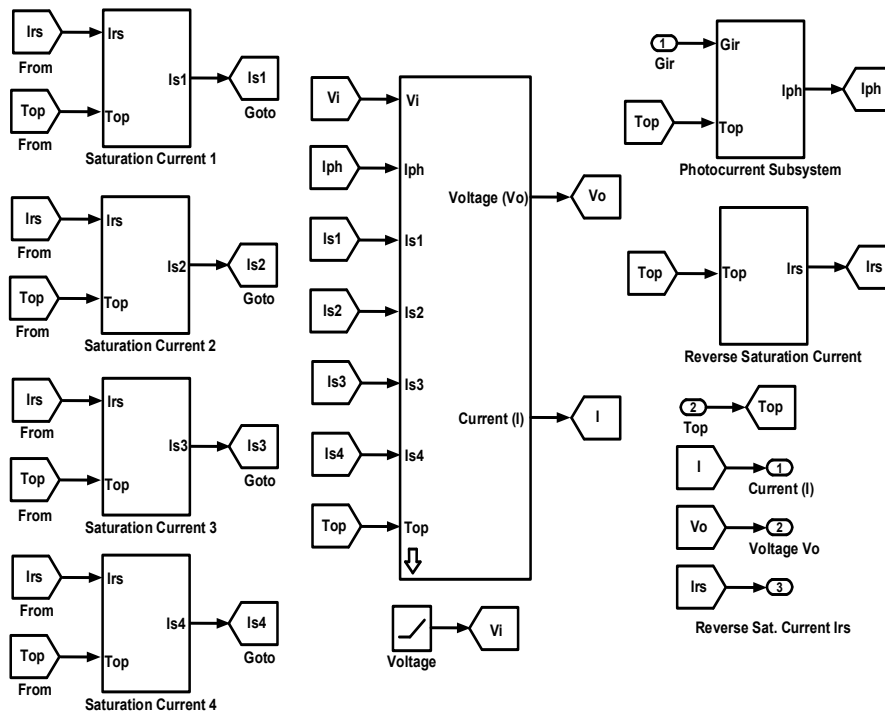


Figure 12. Complete sub-system model of proposed four diode PV cell

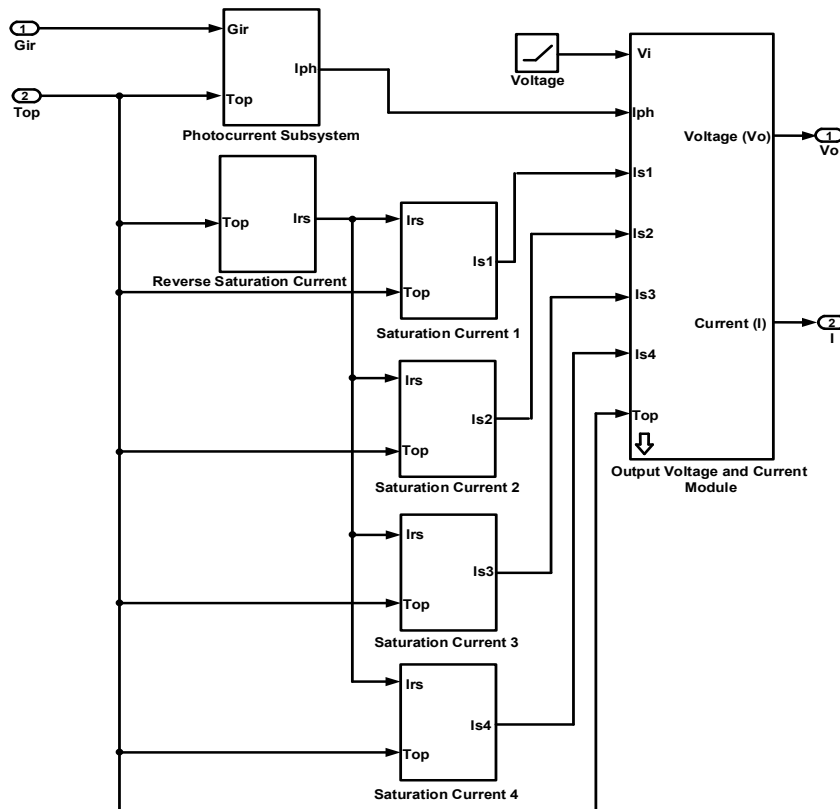


Figure 13. Module output voltage and current of proposed four diode PV cell

5. Results and Discussion

The analysis of mathematical models for single, double, triple, and quadruple diodes solar cells was conducted, and equations were derived based on Kirchhoff's law.

The modeling of the solar PV panel was simulated via MATLAB/Simulink. The characteristics of the PV solar module are presented in Table 1. Table 2 presents the recorded values of the proposed models, including the single, double, triple, and quadruple diode models.

Table 1. Specifications for PV panel

Parameters	Value
Input Power (P_{IN})	1410 W
Maximum Voltage (V_{MPP})	26.3 V
Maximum Current (I_{MPP})	7.61 A
Maximum Power (P_{MPP})	200 W
Short Circuit Current (I_{SC})	8.21 A
Open Circuit Voltage (V_{OC})	32.9 V
Series Resistance (R_{Se})	0.32 Ω
Parallel Resistance (R_{pa})	300 Ω
Total number of series cells (N_{Se})	54
Total number of parallel cells (N_{pa})	1
Voltage Temperature coefficient (K_v)	-123 mV/ $^{\circ}$ C
Voltage Temperature coefficient (K_{SC})	3.18 mA/ $^{\circ}$ C

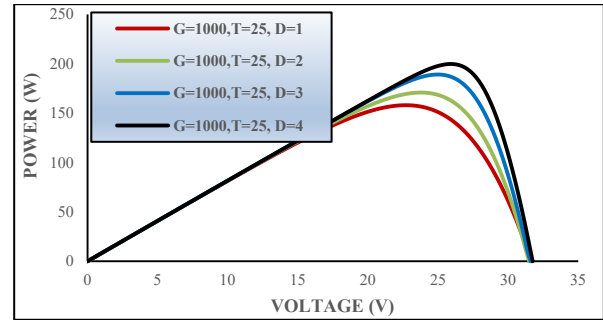
Table 2. Calculated values of proposed single, double, triple and quadruple diode models at STC

Parameters	Single diode Model	Double diode Model	Triple diode Model	Quadruple diode Model
Input Power (P_{IN})	1410 W	1410 W	1410 W	1410 W
Maximum Power (P_{MPP})	159.4 W	170.83 W	173.85 W	199.73 W
Maximum Voltage (V_{MPP})	22.8 V	23.8 V	21.6 V	26 V
Maximum Current (I_{MPP})	6.99 A	7.1775 A	8.038 A	7.68 A
Open Circuit Voltage (V_{OC})	31.7 V	32.9 V	32.9 V	32.9 V
Short Circuit Current (I_{SC})	8.21 A	8.21 A	8.21 A	8.21 A
Diode Ideality Factor (C)	$C_1=2.5$	$C_1=1, C_2=2.2$	$C_1=1, C_2=1.5, C_3=1.3$	$C_1=0.3, C_2=0.5, C_3=0.7, C_4=1$
Series Resistance (R_{Se})	0.32 Ω	0.32 Ω	0.32 Ω	0.32 Ω
Parallel Resistance (R_{pa})	300 Ω	300 Ω	300 Ω	300 Ω
Voltage Temperature coefficient (K_v)	-123 mV/ $^{\circ}$ C	-123 mV/ $^{\circ}$ C	-123 mV/ $^{\circ}$ C	-123 mV/ $^{\circ}$ C
Voltage Temperature coefficient (K_{SC})	3.18 mA/ $^{\circ}$ C	3.18 mA/ $^{\circ}$ C	3.18 mA/ $^{\circ}$ C	3.18 mA/ $^{\circ}$ C

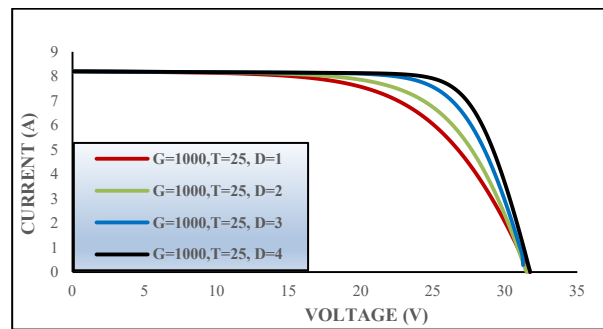
5.1. Constant Radiation and Constant Temperature Conditions

Modeling PV cells by using multiple diodes, the I-V and P-V characteristics of the PV system were investigated under constant temperature conditions at 25°C, with a fixed incident irradiation of 1000W/m². The P-V characteristic has been illustrated in Figure 14(a) and I-V characteristic has been presented in Figure 14(b). Figure (14) showed that when the number of diodes is increased, there is an increase in both the output voltage and the current, which yields the maximum power output of the PV system.

Table 3 illustrates the maximum voltage, maximum power, and maximum current that are increased by large amounts with increasing the number of diodes for both P-V and I-V characteristics models.



(a). Output P-V



(b). Output I-V

Figure 14. Output characteristics of PV under fixed radiation and fixed temperature

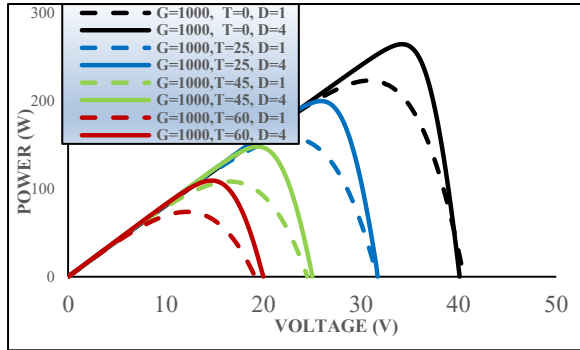
Table 3. Comparison between the number of diodes for fixed values of irradiance and temperature

Solar radiation (W/m ²)	Temp. ($^{\circ}$ C)	Multi diode	Pmp (W)	Vmp (V)	Imp (A)
G=1000	T=25	Single diode, D=1	158.02	22.8	6.931
G=1000	T=25	Double diode, D=2	170.83	23.8	7.177
G=1000	T=25	Triple diode, D=3	189.08	25	7.563
G=1000	T=25	Quadruple diode, D=4	199.73	26	7.682

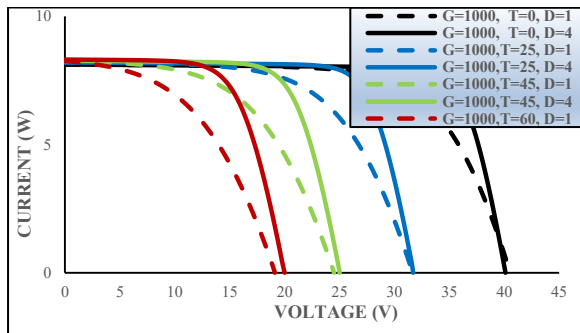
5.2. Constant Radiation and Varying Temperature Conditions

The I-V and P-V characteristics of a single and quadruple diodes, were evaluated at different temperatures while keeping the irradiation at 1000 W/m², the temperatures considered were 0°C, 25°C, 45°C and 60°C, and the obtained results showed that an increase in temperature led to a decrease in both the output current and voltage from the PV module. Consequently, the power output and efficiency of the system also decreased with an increase in temperature.

Figure 15 depicts the I-V and P-V characteristics of the analyzed PV system. Table 4 illustrates that the maximum power, maximum voltage, and maximum current that are increased by large amounts with increasing the number of diodes for both P-V and I-V characteristics models.



(a). Output P-V



(b). Output I-V

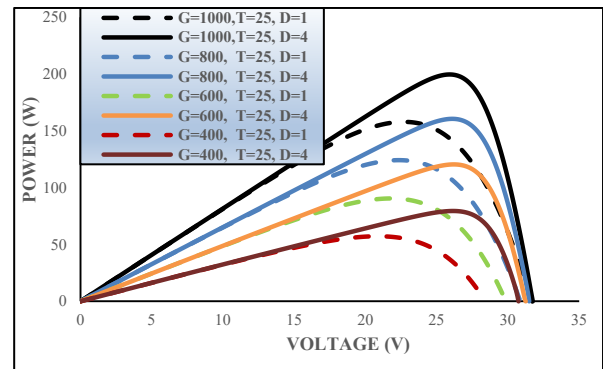
Figure 15. Output characteristics of PV under fixed radiation and variable temperature

Table 4. Comparison between the single and quadruple diodes for fixed values of irradiance and variable temperature

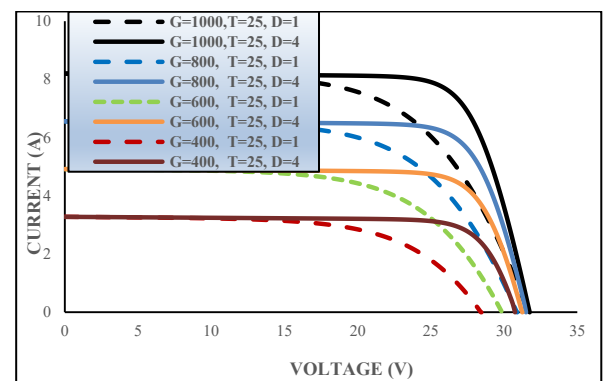
Solar radiation (W/m ²)	Temp. (°C)	Multi diode	Pmp (W)	Vmp (V)	Imp (A)
G=1000	T=0	Single diode, D=1	223.14	30.8	7.245
G=1000	T=0	Quadruple diode, D=4	264.46	34.13	7.75
G=1000	T=25	Single diode, D=1	158.02	22.8	6.93
G=1000	T=25	Quadruple diode, D=4	199.73	26	7.68
G=1000	T=45	Single diode, D=1	108.19	16.6	6.52
G=1000	T=45	Quadruple diode, D=4	147.82	19.4	7.62
G=1000	T=60	Single diode, D=1	73.69	12.2	6.041
G=1000	T=60	Quadruple diode, D=4	109.3	14.6	7.48

5.3. Variable Radiation and Constant Temperature Conditions

During variable radiation conditions on the P-V curve, the power output from the PV system fluctuates with changes in solar radiation levels. The MPP on the P-V curve shifts as radiation intensity varies, potentially leading to changes in the curve's shape. On the other hand, when temperature remains constant and under variable radiation conditions on the I-V curve, the generated current from the PV system remains stable. However, fluctuations in radiation intensity cause variations in the current magnitude, influencing the position and shape of the I-V curve. Figure 16 shows the I-V and P-V characteristics of the analyzed PV system under variable radiation and constant temperature. Table 5 demonstrates a substantial increase in the maximum voltage, maximum power, and maximum current with the inclusion of more diodes in both the P-V and I-V characteristics models.



(a). Output P-V



(b). Output I-V

Figure 16. Output characteristics of PV under variable radiation and fixed temperature

Table 5. Comparison between the single and quadruple diodes for variable values of irradiance and fixed temperature

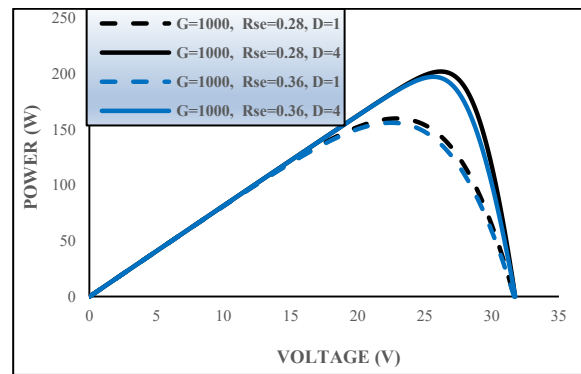
Solar radiation (W/m ²)	Temp. (°C)	Multi diode	Pmp (W)	Vmp (V)	Imp (A)
G=1000	T=25	Single diode, D=1	158.02	22.8	6.93
G=1000	T=25	Quadruple diode, D=4	199.73	26	7.68
G=800	T=25	Single diode, D=1	124.31	22.6	5.55
G=800	T=25	Quadruple diode, D=4	160.67	26	6.18
G=600	T=25	Single diode, D=1	90.58	21.8	4.16
G=600	T=25	Quadruple diode, D=4	120.56	26.2	4.60
G=400	T=25	Single diode, D=1	57.3	21	2.76
G=400	T=25	Quadruple diode, D=4	79.55	26.2	3.04

5.4. Constant Radiation and Varying Series Resistance Conditions

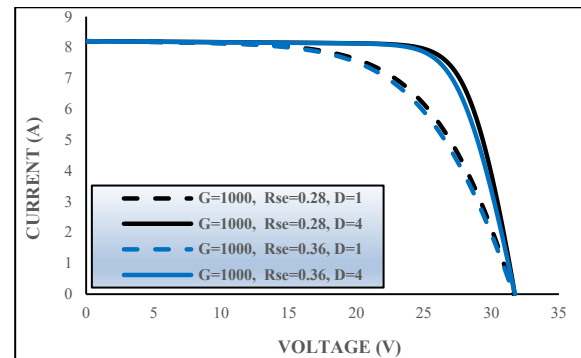
Under constant radiation conditions on the P-V curve, the solar radiation level remains unchanged, resulting in a relatively stable overall shape and position of the P-V curve. However, variations in the series resistance can cause the MPP of the P-V curve to shift, leading to changes in the peak power output of the PV system.

A higher series resistance can lead to reduced efficiency, resulting in a lower maximum power point. Changes in series resistance have an impact on the I-V curve by altering the relationship between current and voltage. An increase in series resistance can cause a decrease in the current generated by the PV system, resulting in a shift in the position of the I-V curve. The magnitude of the current at different voltage points on the curve can be influenced by variations in series resistance.

Figure 17 illustrates the I-V and P-V characteristics of the analyzed PV system under constant radiation and varying series resistance conditions. Table 6 illustrates a significant rise in the maximum voltage, maximum power, and maximum current when incorporating more diodes in both the P-V and I-V characteristics models.



(a). Output P-V



(b). Output I-V

Figure 17. Output characteristics of PV under fixed radiation and variable series resistance

Table 6. Comparison between the single and quadruple diodes for fixed values of irradiance and variable series resistance

Solar radiation (W/m ²)	Resistance (Ω)	Multi diode	Pmp (W)	Vmp (V)	Imp (A)
G=1000	Rse=0.28	Single diode, D=1	159.96	23	6.95
G=1000	Rse=0.28	Quadruple diode, D=4	202.13	26.2	7.715
G=1000	Rse=0.36	Single diode, D=1	156.09	22.6	6.91
G=1000	Rse=0.36	Quadruple diode, D=4	197.38	25.6	7.71

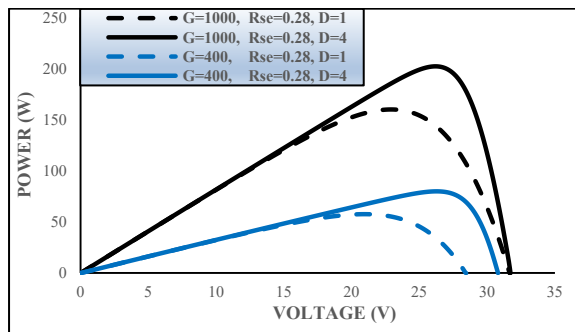
5.5. Variable Radiation and Constant Series Resistance Conditions

During variable radiation conditions on the P-V curve, the power output from the PV system varies with changes in solar radiation levels. The MPP on the P-V curve shifts in response to the varying radiation intensity, potentially altering the curve's shape. Nevertheless, as the series resistance remains constant, changes in the internal resistance do not directly impact the overall position and characteristics of the P-V curve.

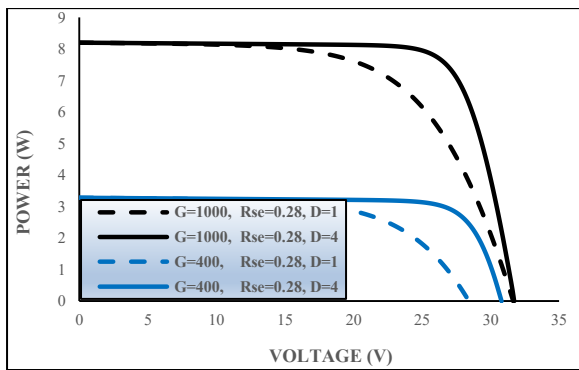
With constant series resistance conditions on the I-V curve, the relationship between current and voltage remains constant. However, fluctuations in radiation intensity affect the magnitude of the current, influencing the position and shape of the I-V curve. Figure 18 illustrates the I-V and P-V characteristics of the analyzed PV system under variable radiation and constant series resistance conditions. Table 7 demonstrates a notable increase in the maximum power, maximum voltage, and maximum current by adding more diodes in both the P-V and I-V characteristics models.

Table 7. Comparison between the single and quadruple diodes for variable fixed values of irradiance and fixed series resistance

Solar radiation (W/m ²)	Resistance (Ω)	Multi diode	Pmp (W)	Vmp (V)	Imp (A)
G=1000	Rse=0.28	Single diode, D=1	159.96	23	6.95
G=1000	Rse=0.28	Quadruple diode, D=4	202.13	26.2	7.715
G=400	Rse=0.36	Single diode, D=1	57.61	21	2.74
G=400	Rse=0.36	Quadruple diode, D=4	79.92	26.2	3.05



(a). Output P-V



(b). Output I-V

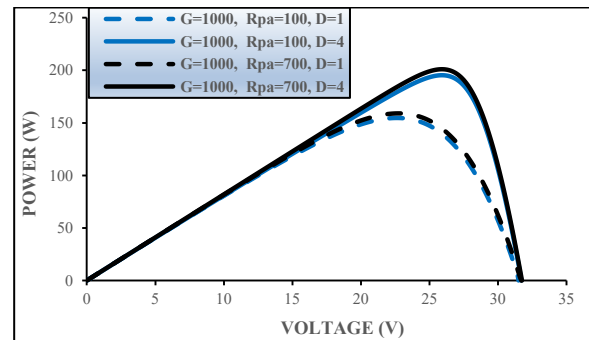
Figure 18. Output characteristics of PV under variable radiation and fixed series resistance

5.6. Constant Radiation and Varying Parallel Resistance Conditions

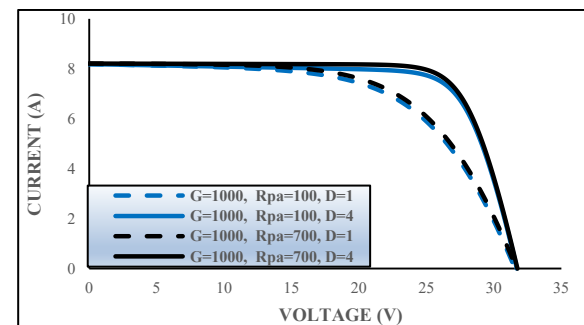
Changes in the parallel resistance value can cause shifts in the MPP on the PV curve, leading to variations in the peak power output of the PV system. The variation in parallel resistance also impacts the I-V curve by altering the current-voltage relationship. An increase in parallel resistance can result in a decrease in the generated current by the PV system, causing the I-V curve's position to shift. The magnitude of the current at different voltage points on the curve can be influenced by changes in parallel resistance. Figure 19 and Table 8 illustrates a significant rise in the maximum voltage, maximum power, and maximum current when incorporating more diodes in both the P-V and I-V characteristics models.

Table 8. Comparison between the single and quadruple diodes for fixed values of irradiance and variable parallel resistance

Solar radiation (W/m ²)	Resistance (Ω)	Multi diode	Pmp (W)	Vmp (V)	Imp (A)
G=1000	Rpa=100	Single diode, D=1	154.64	22.6	6.84
G=1000	Rpa=100	Quadruple diode, D=4	195.3	26	7.51
G=1000	Rpa=700	Single diode, D=1	159	23	6.97
G=1000	Rpa=700	Quadruple diode, D=4	201	26	7.73



(a). Output P-V



(b). Output I-V

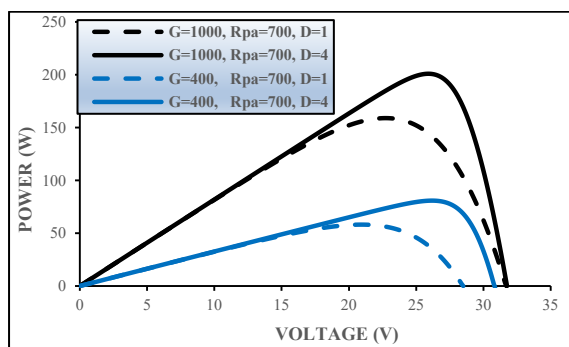
Figure 19. Output characteristics of PV under fixed radiation and variable parallel resistance

5.7. Variable Radiation and Constant Parallel Resistance Conditions

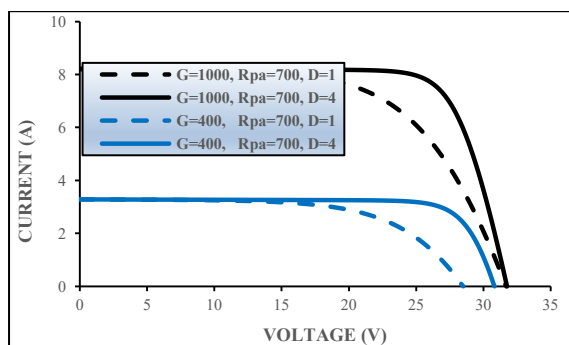
During variable radiation conditions on the P-V curve, the power output from the PV system varies in response to changes in solar radiation levels. The MPP on the P-V curve shifts with fluctuations in radiation intensity, potentially altering the curve's shape. However, these changes in radiation intensity also affect the magnitude of the current, leading to variations in the position and shape of the I-V curve. Table 9 and Figure 20 demonstrates a substantial increase in the maximum power, maximum voltage, and maximum current by adding more diodes in both the I-V and P-V characteristics models.

Table 9. Comparison between the single and quadruple diodes for variable values of irradiance and fixed parallel resistance

Solar radiation (W/m ²)	Temp. (°C)	Multi diode	Pmp (W)	Vmp (V)	Imp (A)
G=1000	Rpa=700	Single diode,D=1	159	23	6.97
G=1000	Rpa=700	Quadruple diode,D=4	201	26	7.73
G=400	Rpa=700	Single diode,D=1	58.13	21	2.77
G=400	Rpa=700	Quadruple diode,D=4	80.86	26.2	3.09



(a). Output P-V



(b). Output I-V

Figure 20. Output characteristics of PV under variable radiation and fixed parallel resistance

6. Conclusion

To facilitate the swift and consistent design of PV modules, the utilization of an efficient, expeditious, and accurate simulator becomes imperative for evaluating the response of the PV cell to rapid or incremental fluctuations in temperature, irradiance, and parasitic resistance. The prevailing methodology for modeling entails the adoption of an equivalent (electrical) circuit that comprehensively encompasses nonlinear as well as linear dynamics. In this investigation, a progressive eleven-parameter quadratic model is introduced for the simulation and representation of a PV unit.

To ascertain the validity and accuracy of the suggested model, the approach was implemented using the specific parameters of PV panels, and the resulting data was meticulously juxtaposed with the observed values derived from the proposed models. Through comprehensive comparative analysis between the quadruple diode model and its counterparts, the single, double, and triple diode models, it has been conclusively established that the quadruple diode model exhibits superior performance and enhanced accuracy and is simulated by MATLAB/Simulink.

Acknowledgements

The authors would like to gratefully acknowledge Al-Iraqia University for supporting the research.

References:

- [1]. Manisalidis, I., Stavropoulou, E., Stavropoulos, A., & Bezirtzoglou, E. (2020). Environmental and health impacts of air pollution: a review. *Frontiers in public health*, 8, 14.
- [2]. Yıldız, İ. (2018). 1.12 Fossil Fuels. *Comprehensive Energy Systems, 1*. Doi: 10.1016/B978-0-12-809597-3.00111-5.
- [3]. El-Dabah, M. A., El-Schiemy, R. A., Hasanien, H. M., & Saad, B. (2023). Photovoltaic model parameters identification using an innovative optimization algorithm. *IET Renewable Power Generation*, 17(7), 1783-1796.
- [4]. Hasan, M. M., Hossain, S., Mofijur, M., Kabir, Z., Badruddin, I. A., Yunus Khan, T. M., & Jassim, E. (2023). Harnessing solar power: a review of photovoltaic innovations, solar thermal systems, and the dawn of energy storage solutions. *Energies*, 16(18), 6456.
- [5]. Kamarulzaman, A., Hasanuzzaman, M., & Rahim, N. A. (2021). Global advancement of solar drying technologies and its future prospects: A review. *Solar Energy*, 221, 559-582.
- [6]. Al-Ezzi, A. S., & Ansari, M. N. M. (2022). Photovoltaic solar cells: a review. *Applied System Innovation*, 5(4), 67.

- [7]. Teh, C. J. Q., Drieberg, M., Soeung, S., & Ahmad, R. (2021). Simple PV modeling under variable operating conditions. *IEEE Access*, 9, 96546-96558.
- [8]. Ebrahimi, S. M., Salahshour, E., Malekzadeh, M., & Gordillo, F. (2019). Parameters identification of PV solar cells and modules using flexible particle swarm optimization algorithm. *Energy*, 179, 358-372.
- [9]. Lo, W. L., Chung, H. S. H., Hsung, R. T. C., Fu, H., & Shen, T. W. (2023). PV Panel Model Parameter Estimation by Using Neural Network. *Sensors*, 23(7), 3657.
- [10]. Toledo, F. J., Galiano, V., Blanes, J. M., Herranz, V., & Batzelis, E. (2023). Photovoltaic single-diode model parametrization. An application to the calculus of the Euclidean distance to an I-V curve. *Mathematics and Computers in Simulation*.
- [11]. Rahman, M. H., Akter, S., & Chowdhury, S. (2023). Evaluation of power performance of solar module using two diode model with MATLAB simulation. *Advanced Journal of Graduate Research*, 13(1), 8-17.
- [12]. Ellithy, H. H., Taha, A. M., Hasanien, H. M., Attia, M. A., El-Shahat, A., & Aleem, S. H. A. (2022). Estimation of Parameters of Triple Diode Photovoltaic Models Using Hybrid Particle Swarm and Grey Wolf Optimization. *Sustainability*, 14(15), 9046.
- [13]. Singh, B., Singla, M. K., & Nijhawan, P. (2022). Parameter estimation of four diode solar photovoltaic cell using hybrid algorithm. *Energy Sources, Part A: Recovery, Utilization, and Environmental Effects*, 44(2), 4597-4613.
- [14]. Fahim, S. R., Hasanien, H. M., Turkey, R. A., Aleem, S. H. A., & Calasan, M. (2022). A comprehensive review of photovoltaic modules models and algorithms used in parameter extraction. *Energies*, 15(23), 8941.
- [15]. Ramadan, A., Kamel, S., Taha, I. B., & Tostado-Véliz, M. (2021). Parameter estimation of modified double-diode and triple-diode photovoltaic models based on wild horse optimizer. *Electronics*, 10(18), 2308.
- [16]. Soliman, M. A., Al-Durra, A., & Hasanien, H. M. (2021). Electrical parameters identification of three-diode photovoltaic model based on equilibrium optimizer algorithm. *IEEE Access*, 9, 41891-41901.
- [17]. Al-Ghezi, M. K., Ahmed, R. T., & Chaichan, M. T. (2022). The Influence of Temperature and Irradiance on Performance of the photovoltaic panel in the Middle of Iraq. *International Journal of Renewable Energy Development*, 11(2), 501.
- [18]. Malik, P., & Chandel, S. S. (2021). A new integrated single-diode solar cell model for photovoltaic power prediction with experimental validation under real outdoor conditions. *International Journal of Energy Research*, 45(1), 759-771.
- [19]. Tifidat, K., Maouhoub, N., Askar, S. S., & Abouhawwash, M. (2023). Numerical procedure for accurate simulation of photovoltaic modules performance based on the identification of the single-diode model parameters. *Energy Reports*, 9, 5532-5544.
- [20]. Senthilkumar, S., Mohan, V., Mangaiyarkarasi, S. P., & Karthikeyan, M. (2022). Analysis of single-diode PV model and optimized MPPT model for different environmental conditions. *International Transactions on Electrical Energy Systems*, 2022.
- [21]. Tifidat, K., Maouhoub, N., & Salah, F. E. A. (2023). Modeling approach for extracting the single-diode model parameters and predicting PV modules performance. In *AIP Conference Proceedings*, 2814(1), AIP Publishing.
- [22]. Osorio, L., Rivera, M., Tuninetti, V., Mediacaja, Y. R., & Wheeler, P. (2023). A MATLAB/GUI for Photovoltaic Modules Performance Simulations Based on Two-Diode Model. *Preprints*, 2023051039.
- [23]. Tifidat, K., Maouhoub, N., Benahmida, A., & Salah, F. E. A. (2022). An accurate approach for modeling IV characteristics of photovoltaic generators based on the two-diode model. *Energy Conversion and Management: X*, 14, 100205.
- [24]. Ridha, H. M., Hizam, H., Mirjalili, S., Othman, M. L., Ya'acob, M. E., & Abualigah, L. (2022). A novel theoretical and practical methodology for extracting the parameters of the single and double diode photovoltaic models. *IEEE Access*, 10, 11110-11137.
- [25]. Singla, M. K., & Nijhawan, P. (2021). Triple diode parameter estimation of solar PV cell using hybrid algorithm. *International Journal of Environmental Science and Technology*, 1-24.
- [26]. Agwa, A. M., Elsayed, S. K., & Elattar, E. E. (2022). Extracting the parameters of three-diode model of photovoltaics using barnacles mating optimizer. *Symmetry*, 14(8), 1569.
- [27]. El-Dabah, M. A., El-Schiemy, R. A., Becherif, M., & Ebrahim, M. A. (2021). Parameter estimation of triple diode photovoltaic model using an artificial ecosystem-based optimizer. *International Transactions on Electrical Energy Systems*, 31(11), e13043.
- [28]. Zaky, A. A., Fathy, A., Rezk, H., Gkini, K., Falaras, P., & Abaza, A. (2021). A modified triple-diode model parameters identification for perovskite solar cells via nature-inspired search optimization algorithms. *Sustainability*, 13(23), 12969.
- [29]. Prakash, S. B., Singh, G., & Singh, S. (2022). Modeling and Performance Analysis of Simplified Three-Diode Photovoltaic Module. *Journal of Electrical Engineering*, 22(1), 55-64.

Appendix A – Nomenclature of variables used in this research

Variable	Description
I_{ph}	light-generated current source in (A)
I_d	diode current in (A)
I_{pa}	parallel resistance current in (A)
V_O	output voltage in (V)
V_{oc}	open-circuit voltage in (V)
V_{MPP_STC}	voltage at maximum power point in (V)
I_{MPP_STC}	current at maximum power point in (A)
P_{MPP}	power at maximum power point in (W)
I	output current in (A)
I_s	diode saturation current in (A)
I_{rs}	diode reverse saturation current in (A)
I_{sc}	short-circuit current in (A)
n	diode ideality factor
V_T	thermal voltage = 26 mV at 300 K
N_{se}	cells connected in series
N_{pa}	cells connected in parallel
K_B	Boltzmann constant, which = $(1.381 \times 10^{-23}$ J/K)
q	Charge of electron, which = $(1.6 \times 10^{-19}$ C)
T_{ref}	reference temperature = 298K
T_{op}	operating temperature
R_{se}	series resistance of a PV, which = 0.32 Ω
R_{pa}	parallel resistance of a PV, which = 300 Ω
G_{pa}	parallel admittance of a PV
E_g	band gap of the silicon, which = 1.1 eV
I_{rsi}	reverse saturation current of i^{th} diode
n_i	ideality factor of i^{th} diode
G_{ir}	the irradiation in (W/m^2)
G_{STC}	the irradiation at standard test condition (STC), which = $1000 W/m^2$
I_{scSTC}	short circuit current of cell at (STC) (in Ampere), which happen with (T=25 short is the cell's short-circuit current temperature coefficient (A/K), which = $-3.18 \text{ mA}/^\circ\text{C}$ and $G=1000 \text{ W}/m^2$)
K_{SC}	short is the cell's short-circuit current temperature coefficient (A/K), which = $-3.18 \text{ mA}/^\circ\text{C}$
K_{ov}	the cell's open-circuit voltage temperature coefficient (V/K), which = $-123 \text{ m V}/^\circ\text{C}$
$[K_{SC}]$, $[K_{ov}]$	normally provided by the manufacturer